 CMES, vol.5, no.1, pp.45-62, 2004

A Lattice Statics-Based Tangent-Stiffness Finite Element Method

Peter W. Chung[1], Raju R. Namburu[2], and Brian J. Henz[3]

Abstract: A method is developed based on an additive modification to the first Lagrangian elasticity tensor to make the finite element method for hyperelasticity viable at the atomic length scale in the context of lattice statics. Through the definition of an overlap region, the close-ranged atomic interaction energies are consistently summed over the boundary of each finite element. These energies are subsequently used to additively modify the conventional material property tensor that comes from the second derivative of the stored energy function. The summation over element boundaries, as opposed to atom clusters, allows the mesh and nodes to be defined independently from the atoms. The method is developed with a specific form of the Tersoff-Brenner potential for carbon. The method correctly predicts the in-plane deformation behavior of a single graphite sheet subjected to displacement boundary conditions. Estimated plane elasticity properties agree with experimental data from the literature. Quenched molecular dynamics results are used to validate the method for homogeneous and inhomogeneous loading constraints.

keyword: Nanomechanics, multiscale modeling, lattice mechanics, continuum mechanics, finite element method.

1 Introduction

The impetus to better understand the mechanics of crystal defects such as dislocations and grain boundaries has led to numerous new developments in multiscale methods. They have been proposed for application to micro devices and to mesoscale material problems; scales in which both atomistic and continuum phenomena need to be resolved [Brenner, Shenderova, Areshkin, and Schall (2002)]. The fundamental idea in these methods is to develop consistent formulations by which both atomic and continuum phenomena can be modeled within a unified framework. Examples include an approach to equilibrate forces between atoms and continua with the continuum region modeled with analytical techniques [Sinclair (1971)]; an atom embedding method inside the finite elements at the FE-atom interface [Mullins and Dokainish (1982)]; a method incorporating a non-local elasticity theory for a transition region connecting the lattice and continuum regions [Kohlhoff, Gumbsch, and Fischmeister (1991)]; an FE-atomistic method with FE properties derived directly from atomistic potentials [Tadmor, Ortiz, and Phillips (1996)]; a method of matched displacements between atomistic molecular dynamics and a micromechanics model [Noguchi and Furuya (1997)]; and a method for dynamically coupling a finite element region to a molecular dynamics region, and still further to a tight-binding region [Broughton, Abraham, Bernstein, and Kaxiras (1999-II)].

In many of the investigations to date, it is common practice to use bulk elasticity in regions far from the defect where strains are small. And conversely, in regions at or close to the defect, lattice statics or molecular dynamics (MD) are employed to capture the detailed lattice scale anharmonic effects. The intrinsic assumption is that the problem under consideration always possesses a boundary far enough away from the defect so that atomic force fields per unit area asymptote to conventional continuum stress definitions. Therefore, the multiscale analyses involve disparate length scales where each scale is asymptotically smaller than the next.

The motivation for this juxtaposition of scales stems from the limitations of each scale-specific method. The finite element method employs constitutive laws that are inappropriate for treating atomistic effects. Yet, the size of the problem is very large and is beyond the reach of lattice statics or molecular dynamics alone. To study problems where both atoms and continuum must be resolved, a unified framework that models both scales is

[1] Corresponding author, Computational and Information Sciences Directorate, U.S. Army Research Laboratory, Aberdeen Proving Ground, MD 21005-5067, pchung@arl.army.mil
[2] U.S. ARL, CISD, APG, MD
[3] U.S. ARL, CISD, APG, MD

needed. Each of the efforts previously described provides a unique methodology for accomplishing this. However, common to all of the methods is a definite interface that separates the atomic region from the continuum region. On one side is the atom region modeled with, say, classical potentials via lattice statics or molecular dynamics. On the other side is the continuum region modeled with, say, the finite element method, which is governed by the standard principles of continuum mechanics. This assumes that in regions close to this interface, both continuum mechanics and atomistic mechanics are valid.

This leads to the question: "How valid is the continuum mechanics-based finite element method at this interface?" It is assumed that the atomistic equations are always more accurate, in a physics sense, than the continuum equations. Therefore, the simple answer to the question is "yes" as long as the atomistic region is always made sufficiently large. But this would result in problems containing many more atoms than are necessary to accurately solve the problem and can also lead to higher computational cost.

The dilemma can be remedied through several approaches that can be found in the literature. One is to establish a transition region deterministically between the atoms and the continuum with a theory such as non-local elasticity [Kroner (1967)] where both atomic and continuum effects are valid [Kohlhoff, Gumbsch, and Fischmeister (1991)]. Another approach is to specify the nonlocal region adaptively [Tadmor, Ortiz, and Phillips (1996)]. A third is to use a fully non-local technique in which finite atom cluster regions are defined around nodes [Knap and Ortiz (2001)]. In these approaches, however, detailed placement of the nodes is necessary so that they coincide with atoms at the interface. Therefore the interface and the shape of the mesh are determined by the kinematic constraints that are needed to tie the atoms to the finite element mesh. The atoms act as nodal anchors for the mesh such that the smallest element size is exactly equal to the length of the primitive lattice vector. A desirable feature for a theory at the interface is to have the capability to define the nodes and elements independently from the atoms yet ensure that the numerical formulations remain faithful to the atoms they represent.

Some related efforts have been undertaken to circumvent the interface entirely through homogenization theory [Chung and Namburu (2003)]. Homogenization methods have been used predominantly in the computational literature for composite structures modeling [Raghavan and Ghosh (2004)] and composites manufacturing modeling (e.g., see Ngo and Tamma (2004)) with considerable success.

A different but related problem is the modeling of nanoscale devices where definable phenomena do not exceed tens of nanometers. Novel materials and structures such as nanotubes and nanowires and some components of microelectromechanical devices (MEMS) possess material and phenomenological characteristics that reside in length scales smaller than the acceptable lower length scale limit of continuum theories. These devices typically span dimensions as small as tens of Angstroms to as large as tens of micrometers. Despite the strength and validity of the finite element method, its reliance on phenomenological constitutive laws based on continuum-scale observations precludes its applicability to the small scale regimes of these devices.

Yet many problems dominated by atomistic effects exhibit continuum-like behavior. An example of this is the nanotube instability problem [Yakobson, Brabec, and Bernholc (1996)]. The localized features of the tubes that are of interest warrant detailed molecular dynamics that render the earlier multiscale methods, namely the treatment of the bulk continuum scales, unnecessary. This is understandable in light of the mesoscale regimes to which these multiscale methods are applied (and for which they were originally developed). To date, continuum-like methods that have been developed for nanoscale devices rely on parameterizations of more detailed calculations, e.g. from molecular dynamics and/or *ab initio*, to be fed into existing continuum models such as shell [Yakobson, Brabec, and Bernholc (1996)] and beam [Wong, Sheehan, and Lieber (1997)] theories. Unfortunately, developments such as these are difficult to extend to general computational methods because of the strict assumptions associated with shell and beam theories.

There is one common issue shared in the two problems discussed thus far, i.e., multiscale modeling and nanoscale device modeling. The methodology needed to treat the interface in each of these types of problems can also be employed for developing continuum based understanding of nanodevices. This is predicated on the assumption that interface modeling entails approximating a small number of atoms with a continuum-like structure and imbuing that structure with the appropriate character-

istics of the atoms. To date, few studies can be found in the literature, particularly in new finite element and other computational methods, that further develop methods for the interface. It is still unclear how to model continua near the interface where a finite element, say, spans a volume occupied by at most five or ten atoms. It is evident from the many molecular dynamics and condensed matter physics investigations in the literature that the insights gained from such studies are potentially very useful.

In this paper, a lattice statics based finite element method that is valid at the so-called interface/transition region is presented. The objective is to develop a method that approximates the non-local behavior of a system as small as one or two atoms to as large as millions of atoms. It is specifically targeted for two types of applications. First, for multiscale methods, the developments presented here should be used in conjunction with bulk finite elements at coarser scales and molecular methods (i.e., lattice statics, molecular dynamics or density functional methods) at finer scales. And second, for studying very small devices where continuum-like phenomena are of interest but containing a number of atoms too small for continuum modeling. The method minimizes the energy over a reduced number of degrees of freedom yet returns the qualitative and quantitative atomistic results correctly. Therefore, it is neither entirely atomistic nor entirely continuum. The method is based on the development of a condensation term that is evaluated and used to correct the atomistic energy. In this sense, it builds upon the work of Knap and Ortiz [Knap and Ortiz (2001)] by introducing level-set regions around the element and computing their energy contribution to the associated element. This energy is subsequently used with the standard hyperelastic constitutive definition to derive the tangent material property tensor by taking second derivatives with respect to the deformation gradient. The constitutive properties are then employed in the partial differential equations that are solved through a standard finite element formulation over the reduced number of degrees of freedom. The presentation of the paper is general for multi-dimensional systems, but to demonstrate the application 2-D examples are shown.

The contents of this paper are as follows. In section 2, the conventional continuum equations are shown eventually leading to a variational form based on the principle of virtual work. In section 3, a corrected stored energy (free energy at zero temperature) function is derived and used to modify the traditional local element energy. This function is summed over the surface of each element and ensures that interactions with atoms exterior to the element are properly included, which leads to the definition of the so-called overlap region. In section 4, the method by which the atomic information is passed to the continuum through the constitutive properties is described. Then in section 5, the numerical implementation details are shown. Examples are used in section 6 to validate the method against lattice statics solutions through quenched molecular dynamics simulations. Discussions and concluding remarks are in section 7.

2 Continuum Formulations

The goal of this section is to formulate the variational equations that form the basic equations for the finite elements consistent with lattice-statics energy. The point of departure from classical continuum mechanics is in the definition of the constitutive law where the first elasticity tensor (using the terminology of Marsden and Hughes (1983)) is defined from the second derivative of the stored energy, and the stored energy is taken from the atomistic potential. This type of approach is due to Kroner (1967), and more recently in a computational setting due to Kohlhoff, Gumbsch, and Fischmeister (1991) and Tadmor, Ortiz, and Phillips (1996). The framework for the continuum equations are developed here and the detailed derivation of the atomistic constitutive relations are developed in the next section.

Let Ω be a bounded domain with boundary Γ. A material point $\mathbf{X} \in \Omega$ deforms to the spatial point $\mathbf{x}$ through the deformation gradient defined by

$$\mathbf{F} = \frac{\partial \mathbf{x}}{\partial \mathbf{X}} = \nabla_0 \mathbf{x}, \tag{1}$$

where ∇_0 signifies the gradient taken with respect to the undeformed configuration. Through the conservation of linear momentum,

$$\nabla_0 \cdot \mathbf{P} + \mathbf{f}_0 = 0, \tag{2}$$

where $\mathbf{P}$ is the first Piola-Kirchoff stress tensor and $\mathbf{f}_0$ is the body force per unit of undeformed volume. In rate form, equation (2) can be written as,

$$\nabla_0 \cdot \dot{\mathbf{P}} + \dot{\mathbf{f}_0} = 0. \tag{3}$$

Then, using the principle of virtual work, equation (3) can be rewritten as

$$\int_\Omega \left(\nabla_0 \cdot \dot{\mathbf{P}}\right) \delta\mathbf{u} d\Omega + \int_\Omega \dot{\mathbf{f}}_0 \cdot \delta\mathbf{u} d\Omega = 0, \quad \forall \delta\mathbf{u}, \tag{4}$$

where $\delta\mathbf{u}$ is the appropriate virtual displacement. Finally, for a unit normal $\mathbf{N}$ such that the surface traction is defined by $\dot{\mathbf{t}} = \dot{\mathbf{P}} \cdot \mathbf{N}$, integrating by parts yields,

$$\int_\Omega \dot{\mathbf{P}} : \nabla_0 \delta\mathbf{u} d\Omega = \int_\Gamma \dot{\mathbf{t}}_0 \cdot \delta\mathbf{u} d\Gamma + \int_\Omega \dot{\mathbf{f}}_0 \cdot \delta\mathbf{u} d\Omega. \tag{5}$$

The definition of hyperelasticity provides the constitutive information of the material as a function of the stored energy W via

$$\mathbf{P} = \frac{\partial W}{\partial \mathbf{F}}, \tag{6}$$

and the first elasticity or Lagrangian elasticity tensor is defined by

$$\boldsymbol{C} = \frac{\partial^2 W}{\partial \mathbf{F} \partial \mathbf{F}} = \frac{\partial \mathbf{P}}{\partial \mathbf{F}}. \tag{7}$$

Note $\boldsymbol{C}$ possesses only major symmetry and lacks the minor symmetries found in its spatial counterpart. To this end, under certain situations, a more careful accounting of the angular momentum balance may be necessary [Atluri (1979, 1980)]. It follows from equation (7) that $\mathbf{P}$ is related to $\mathbf{F}$ through

$$\dot{\mathbf{P}} = \boldsymbol{C} : \dot{\mathbf{F}} \tag{8}$$

where

$$\dot{\mathbf{F}} = \partial \dot{\mathbf{u}} / \partial \mathbf{X} = \partial \mathbf{v} / \partial \mathbf{X}, \tag{9}$$

and where $\dot{\mathbf{u}} = \mathbf{v}$ denotes the velocity. Substituting equations (7), (8) and (9) into equation (5) finally leads to

$$\begin{aligned} &\int_\Omega \left(\nabla_0 \delta\mathbf{u}\right)^T : \frac{\partial^2 W}{\partial \mathbf{F} \partial \mathbf{F}} : \left(\nabla_0 \mathbf{v}\right) d\Omega \\ &\quad = \int_\Gamma \dot{\mathbf{t}}_0 \cdot \delta\mathbf{u} d\Gamma + \int_\Omega \dot{\mathbf{f}}_0 \cdot \delta\mathbf{u} d\Omega, \quad \forall \delta\mathbf{u}. \end{aligned} \tag{10}$$

It is quite clear that equation (10) is the standard variational form for an elliptic partial differential equation. In the next section, the atomistic part of the developments will be explained. Then in section 4, the method for combining the two will be described.

3 Atomistic Definitions

A key assumption in this paper is the Cauchy-Born approximation [Ericksen (1984)], which assumes that the homogeneous deformation of the lattice gives the energy minimizing configuration of the deformed atoms. In the finite element context, this means that within each element the atoms deform homogeneously (see Figure 2). The positions of the atoms are denoted by their Cartesian coordinates $\mathbf{X}$ such that atom i is located at $\mathbf{X}_{(i)}$. The displacement of atom i is $\mathbf{q}_{(i)}$ such that upon deformation, the new position is given by

$$\mathbf{x}_{(\mathbf{i})} = \mathbf{X}_{(\mathbf{i})} + \mathbf{q}_{(\mathbf{i})}. \tag{11}$$

The deformation gradient is defined by

$$\mathbf{F} = \frac{\partial \mathbf{x}}{\partial \mathbf{X}}. \tag{12}$$

The vector $\mathbf{R}$ separating two atoms i and j in the reference configuration is given by

$$\mathbf{R}_{(ij)} = \mathbf{X}_{(j)} - \mathbf{X}_{(i)}. \tag{13}$$

The vector $\mathbf{r}$ separating two atoms in the deformed configuration is given by

$$\mathbf{r}_{(ij)} = \mathbf{x}_{(j)} - \mathbf{x}_{(i)}. \tag{14}$$

Then the Cauchy-Born approximation states that the distance between atoms in their minimizing configuration is given by

$$\begin{aligned} \mathbf{r}_{(ij)} &= \mathbf{F}\mathbf{X}_{(j)} - \mathbf{F}\mathbf{X}_{(i)} \\ &= \mathbf{F}\mathbf{R}_{(ij)}. \end{aligned} \tag{15}$$

Although the present focus is on planar sheets, one might use a more general exponential mapping procedure like the one described by Arroyo and Belytchko (2002). Ultimately, like the Cauchy Born approximation, this is still an approximation to the more general case in which all atoms are free to move independently.

The energy associated with the deformation of the atoms is modeled using the so-called type II parameterization of the Tersoff-Brenner potential [Tersoff (1988); Brenner (1990)]. In this work, higher order conjugation terms are omitted. This effectively removes third nearest neighbor atomic interactions that are mainly used in problems such as phase change where the local force field environment around the second nearest neighbor atom is necessary. For a simple hyperelastic atomistic-continuum

method, the qualitative ratio of contribution to computational complexity for including these interactions is very small and are therefore presently excluded. However, the extension of the present method to account for these terms is immediately obvious. Additional details on these excluded terms can be found in Brenner (1990).

The stored energy form of the Tersoff-Brenner potential is,

$$W = \frac{1}{n}\left[E_b(\mathbf{x}) - E_b(\mathbf{X})\right], \tag{16}$$

where W is the energy density of the frozen system, n is the number of atoms, and E_b is the binding energy for a pure carbon system. From Brenner (1990), the energy is given as

$$E_b(\mathbf{r}) = \sum_i \sum_{j(>i)} \left[V_R\left(r_{(ij)}\right) - \overline{B} V_A\left(r_{(ij)}\right)\right], \tag{17}$$

which has repulsive and attractive terms, respectively,

$$V_R(r) = \frac{f_{(ij)}(r) D^{(e)}}{(S-1)} e^{-\sqrt{2S}\beta(r-R^{(e)})}, \tag{18}$$

$$V_A(r) = \frac{f_{(ij)}(r) D^{(e)} S}{(S-1)} e^{-\sqrt{\frac{2}{S}}\beta(r-R^{(e)})}, \tag{19}$$

a bond order term that accounts for the local environment of each atom

$$\overline{B} = \frac{1}{2}\left(B_{(ij)} + B_{(ji)}\right), \tag{20}$$

$$B_{(ij)} = \left[1 + \sum_{k(\neq i,j)} G(\theta_{(ijk)}) f_{(ik)}\left(r_{(ik)}\right)\right]^{-\delta}, \tag{21}$$

$$G(\theta) = a_o\left\{1 + \frac{c_o^2}{d_o^2} - \frac{c_o^2}{d_o^2 + (1+\cos\theta)^2}\right\}, \tag{22}$$

and the cut-off function which limits the range of the interactions

$$f_{(ij)}(r) = \begin{cases} 1, & r < R^{(1)} \\ \frac{1}{2} + \frac{1}{2}\cos\left[\frac{\pi(r-R^{(1)})}{(r-R^{(2)})}\right], & R^{(1)} < r < R^{(2)} \\ 0, & r > R^{(2)} \end{cases}, \tag{23}$$

The constants are given in Table 1.

As a result of equation (23), equation (16) is an absolutely and uniformly convergent series with a convergence radius of $R^{(2)}$, i.e., the cut-off distance. This radius can be used as a condensation parameter that defines a closed region in which atoms external to an element determines the energy within the element. Energy modifying terms in a periodic molecular cell to account for long-range interactions have been studied in Madelung (1918) and Ewald (1921), and more recently in DeLeeuw, Perram, and Smith (1980) and Heyes (1981) with additional references therein. The concept of employing modifying terms to the energy in this paper are due to these earlier investigations. For the specific case of graphene, the convergence factor extending beyond the boundaries of each element creates "overlap" regions. All atoms in the overlap have a non-negligible contribution to the local element energy W^h.

Table 1 : Parameters for Tersoff-Brenner potential.

$R^{(e)}$	1.39 Å
$D^{(e)}$	6.0 eV
S	1.22
β	2.1 Å
δ	0.5
$R^{(1)}$	1.7 Å
$R^{(2)}$	2.0 Å
a_o	0.00020813
c_o^2	330^2
d_o^2	3.5^2

For the sake of discussion, it is useful to express the potential in equation (16) in the following way:

$$E_b = \sum_i \left\{ \sum_{j(>i)} \left[\phi\left(r_{(ij)}\right) + \sum_{k(\neq i,j)} \left[\psi\left(\mathbf{r}_{(ij)}, \mathbf{r}_{(ik)}\right) + \psi\left(\mathbf{r}_{(ji)}, \mathbf{r}_{(jk)}\right)\right]\right] \right\}, \tag{24}$$

such that

$$E_b = \sum_i \sum_{j(>i)} E_{(ij)} + \sum_i \sum_{j(>i)} \sum_{k(\neq i,j)} E_{(ijk)}. \tag{25}$$

The Tersoff-Brenner potential [Brenner (1990)] possesses a bond order term that can be expressed in the form shown in the k-summation term in equation (24). Any subtended angle $\theta_{(ijk)}$ created by two vectors $\mathbf{r}_{(ij)}$ and $\mathbf{r}_{(ik)}$ can be obtained from the inner product of the two vectors divided by their magnitudes.

In the next section, the details of integrating atomistic and continuum descriptions are shown. Typically, this entails equating the atomistic energy to the free energy of the solid under a zero temperature condition. However, due to the finite element context, additional considerations are needed.

4 Multiscale: Atoms and Continuum

There are two approaches for joining or linking such that information can be exchanged between atomistic and continuum regions. The first is to generate the mesh based on the positions of the atoms such that each node along an edge of the mesh coincides with an atom at the edge of the lattice. This allows irreducible variables such as displacements and velocities to be passed from one region to the next. Problems involving the exchange of irreducible variables generally contain distinct atomistic and continuum regions with a definitive interface shared between them. The second is to develop the constitutive properties (a reducible variable used in context with stresses and strains) for the continuum from the atomistic potential. As a consequence of using reducible variables, an atomistic region need not be defined separately from a continuum region. Therefore kinematic linking is unnecessary. The domain of a typical problem using this approach generally contains only a continuum but has an underlying lattice that is not modeled explicitly. The second method is commonly accompanied in the literature with liberal use of translation invariant properties of the lattice (e.g. see Chung and Namburu (2003)). Translation invariance is necessary to give rise to continuum models such as bulk elasticity.

The goal is to develop a method that is a combination of both approaches. Although the atomic degrees of freedom are not modeled explicitly, as in lattice statics, the atom positions are used with no assumption of translation invariance. In the following, first the finite element equations are derived in the context of hyperelasticity. Then, the modifications to the atomistic energy, namely the lattice sums, are made that make the formulation energetically consistent over finite elements.

4.1 Continuum: Finite Elements

The aim here is to replace equation (10) with an approximate energetically consistent finite element form. To do this, approximate this problem with the simplest finite element method using piecewise linear functions. Take $\overline{\Omega} = \Omega \cup \partial\Omega$ and let $\Omega_h = \bigcup_e \Omega^e \subset \overline{\Omega}$ with

$$\gamma r_o < h \leq h_o \text{ and } 0 < \gamma < 1 \tag{26}$$

be a finite number of closed elements with disjointed but conforming interiors. The parameter γ is adjustable so that it restricts the smallest allowable element size, h, and ensures that each element circumscribes at least one atom (represented by the nearest neighbor distance, r_o) leaving no "vacuous" gaps in the mesh, i.e., the "smallness" of the elements is restricted. With this discretization, equation (10) takes the new approximate form

$$\begin{aligned} &\int_\Omega \left(\nabla_0 \delta\mathbf{u}^h\right)^T : \frac{\partial^2 W^h}{\partial\mathbf{F}\partial\mathbf{F}} : \left(\nabla_0 \mathbf{v}^h\right) d\Omega \\ &\quad = \int_{\partial\Omega} \dot{\mathbf{t}}_0 \cdot \delta\mathbf{u}^h d\Gamma + \int_\Omega \dot{\mathbf{f}}_0 \cdot \delta\mathbf{u}^h d\Omega, \qquad \forall \delta\mathbf{u}^h \end{aligned} \tag{27}$$

where the script h denotes the finite element approximation. Then, in the usual manner, let

$$\delta\mathbf{u}^h = \sum_a c_a N_a, \tag{28}$$

$$\mathbf{v}^h = \sum_a v_a N_a, \tag{29}$$

where a runs over all node numbers, c_a is a constant, N_a is the shape function associated with node a and v_a is the unknown velocity at node a. Let $\mathbf{B}_a = \nabla_0 N_a$. Then, for all c_a, the following must hold:

$$\begin{aligned} &\sum_e \int_{\Omega^e} \frac{\partial^2 W^h}{\partial\mathbf{F}\partial\mathbf{F}} : (\mathbf{B}_a \otimes \mathbf{B}_b)\, v_b d\Omega \\ &\quad = \int_\Gamma \dot{\mathbf{t}}_0 N_a d\Gamma + \int_\Omega \dot{\mathbf{f}}_0 N_a d\Omega. \end{aligned} \tag{30}$$

In the continuum finite element approximation (for hyperelasticity, in particular), it is commonly acceptable to take W^h uniform over all elements Ω^e. For a crystal or small crystallite, this is generally untrue. This has been illustrated quite clearly in Shenoy (1999) in the manifestation of so-called ghost forces. For now, it is clear these observations indicate the problem has both geometric and material nonlinearity. It remains to define W^h more precisely for material nonlinearity in the next section. Careful accounting of the local definition of W^h is needed to ensure a finite element energy consistent with the underlying atoms each element is meant to approximate. The geometric nonlinearity can be treated using numerous standard techniques. In this work, an updated Lagrangian formulation is used.

4.2 Atomistic: Lattice Sums

Assume that the modification of W^h is

$$W^h = W^e + W^e_{\text{overlap}}, \tag{31}$$

where W^e is the local energy of the element and W^e_{overlap} is half of the energy contained in the overlap. The union of the element and overlap regions is the region over which the condensation is performed.

For the set of all atoms A, define the atoms within each element by A^e such that $A = \bigcup_e A^e$. Define a region $\Omega^e_{\text{overlap}} \subset \overline{\Omega}$ and let $A^e_{\text{overlap}} \subset A$ be the set of all atoms in $\Omega^e_{\text{overlap}}$, and likewise, let $A^e \subset A$ be the set of atoms in Ω^e. Note that, in general, $\Omega^e_{\text{overlap}}$ is not a simply connected domain, and in general, $A^e \cap A^e_{\text{overlap}} \neq \emptyset$. Figure 1 depicts these regions for a single four-noded element. The region of width $2R^{(2)}$ is the overlap region.

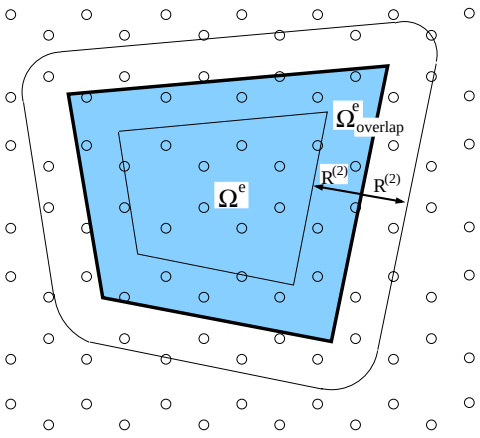

Figure 1 : An element Ω^e and its associated overlap region $\Omega^e_{\text{overlap}}$.

The atom indices in the original potential defined in equations (17)–(22), i.e., in the absence of any finite element approximation, are defined by

$$W = W \begin{cases} i \in \{A\} \\ j \in \{A, > i\} \\ k \in \{A, \neq i, j\}. \end{cases} \tag{32}$$

With the finite element approximation, W is now approximated by W^h locally within each element and the indices must therefore be changed. From equation (31), the new atom indices are defined by

$$\begin{aligned} W^e &= W \begin{cases} i \in \{A^e\} \\ j \in \{A^e, > i\} \\ k \in \{A^e, \neq i, j\}. \end{cases} \quad \text{and} \\ W^e_{\text{overlap}} &= \frac{1}{2} W \begin{cases} i \in \left\{A^e \cap A^e_{\text{overlap}}\right\} \\ j \in \left\{A^e_{\text{overlap}} \backslash A^e, > i\right\} \\ k \in \{A^e, \neq i, j\}. \end{cases} . \end{aligned} \tag{33}$$

The factor of $1/2$ in equation (33) is needed to avoid double counting the overlap energy in adjacent elements. W^e and W^e_{overlap} now form the components of equation (31), the energy of the finite element. In the next section, the second derivative of this energy is used to estimate the new effective first Lagrangian elasticity tensor.

4.3 Derivatives of the Potential

The first derivative of the strain energy gives the first Piola-Kirchoff stress and the second gives the first Lagrangian elasticity tensor. By equating the atomistic potential with the strain energy as in section 4.2, the stresses and constitutive properties can be obtained from atomistic variables. The derivatives are first obtained with respect to the fundamental variables of the potential, which are the interatom vectors. Then, the chain rule yields appropriate derivatives with respect to the gradients. The details for the calculation of the Tersoff-Brenner potential are provided in the appendix and only general forms are presented here.

The first Piola-Kirchoff stress is given by

$$\begin{aligned} \mathbf{P} &= \frac{\partial W}{\partial \mathbf{F}} \\ &= \frac{1}{n} \frac{\partial E_b}{\partial \mathbf{F}}, \end{aligned} \tag{34}$$

and using equation (25) with the the chain rule for derivatives, it is

$$\begin{aligned} \mathbf{P} =& \frac{1}{n} \frac{\partial E_b}{\partial \mathbf{F}} \\ =& \frac{1}{n} \sum_i \sum_{j(>i)} \frac{\partial E_{(ij)}}{\partial \mathbf{r}_{(ij)}} \frac{\partial \mathbf{r}_{(ij)}}{\partial \mathbf{F}} \\ &+ \sum_i \sum_{j(>i)} \sum_{k(\neq i,j)} \left(\frac{\partial E_{(ijk)}}{\partial \mathbf{r}_{(ij)}} \frac{\partial \mathbf{r}_{(ij)}}{\partial \mathbf{F}} \right. \\ &\left. + \frac{\partial E_{(ijk)}}{\partial \mathbf{r}_{(ik)}} \frac{\partial \mathbf{r}_{(ik)}}{\partial \mathbf{F}} + \frac{\partial E_{(ijk)}}{\partial \mathbf{r}_{(jk)}} \frac{\partial \mathbf{r}_{(jk)}}{\partial \mathbf{F}} \right). \end{aligned} \tag{35}$$

The expression of the atomistic energy E_b contains only the deformed component, i.e., $E_b(\mathbf{x})$ in equation (16). The derivative $\partial E_b(\mathbf{X})/\partial \mathbf{F}$ is zero.

Using a similar approach with an additional derivative yields the first Lagrangian elasticity tensor. This is the traditional way of estimating the elastic properties of lattices. The algebraic details are shown in the appendix.

$$\frac{\partial^2 W}{\partial \mathbf{F}\partial \mathbf{F}} = \frac{1}{n}\frac{\partial^2 E_b}{\partial \mathbf{F}\partial \mathbf{F}} \tag{36}$$

The first Lagrangian elasticity tensor (36) is used as the material property tensor in equation (30) subject to the modification of equation (31).

5 Implementation

The details of the numerical implementation of the method is presented in this section. All loads and boundary conditions are applied directly to the mesh. Atoms contribute to the problem only through the modified material property tensor. Therefore, energy is minimized only over nodal degrees of freedom.

The finite element method uses a standard implicit solution procedure at each incremental load step with an updated Lagrangian formulation to update the mesh at each step. The stiffness matrix is assembled on an element by element basis using a second order numerical quadrature rule. From equation (30), the quadrature rule for each element stiffness matrix $\mathbf{K}_{ab}$ is computed by

$$\begin{aligned}\mathbf{K}_{ab} &= \int_{\Omega^e} \frac{\partial^2 W^h}{\partial \mathbf{F}\partial \mathbf{F}} : (\mathbf{B}_a \otimes \mathbf{B}_b)\, d\Omega \\ &= \sum_{r=1}^{2}\sum_{s=1}^{2} w(r,s)\frac{\partial^2 W^h}{\partial \mathbf{F}\partial \mathbf{F}} : (\mathbf{B}_a(r,s) \otimes \mathbf{B}_b(r,s)),\end{aligned} \tag{37}$$

where r and s run over the order of the quadrature rule, $w(r,s)$ are the quadrature weights and $\mathbf{B}(r,s)$ is the matrix containing derivatives of the shape functions evaluated at the quadrature points. The second derivative of W^h is presently assumed constant in each element, Ω^e, but is a nonlinear function of the position of the atoms. Newton iterations are presently used to handle this nonlinearity.

The solution follows a standard finite element method update procedure. It is based on quasistatic load increments with nonlinear material iterations, or quenching iterations in a molecular dynamics sense. An iterative conjugate gradient solver is presently used for the implicit solution procedure and Newton iterations are used for the nonlinear iterations. The algorithm is as follows:

for *loadstep* $= 1$ to *maxloadstep* **do**
  for *quenchstep* $= 1$ to *maxquenchstep* **do**
    for all *elements* **do**
      compute $\partial^2 W^h/\partial \mathbf{F}^2$
      assemble $\mathbf{K}$
    end for
    apply incremental nodal constraints and/or loads
    solve $\mathbf{K}\Delta\mathbf{u} = \mathbf{f}$
    update iterative atom positions
    test convergence
  end for
  update mesh $\mathbf{X}_a = \mathbf{X}_a + \Delta\mathbf{u}$
  update atom positions
  compute new atomistic energy
end for

An additional algorithm is used inside the element loop to search in a cluster of atoms for those atoms that are inside the element and overlap regions, respectively. The size of the cluster is determined in the first load step and stored for use in subsequent steps. The search procedure is based on an algorithm due to Eberly (2002) that finds the distance between a point and a triangle in a plane. In the search algorithm, the quadrilateral is constructed from two triangles.

Within each quench iteration, the atom positions are updated using equation (39) on an element-by-element basis. This results in atom deformation patterns like the one depicted schematically in Figure 2. The overlap region for the center element encompasses atoms in adjacent elements that, when combined, are not in a homogeneous deformation pattern.

6 Examples

In this section, several results are validated with lattice statics solutions that are obtained through quenched molecular dynamics simulations that employ the Tersoff potential [Tersoff (1988); Rifkin (2002)]. Planar problems are considered to demonstrate the method without loss of generality. The formulations can be extended readily to more complicated 3-D systems. Fixed displacement conditions are used in each example. The

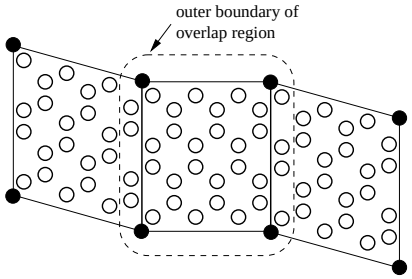

Figure 2 : Deformation is homogeneous in each element but inhomogeneous with overlap region included.

problem is of a graphene sheet one atom thick. The conditions are illustrated schematically in Figure 3. Two load cases are considered along one edge of the sheet: I) a uniform displacement condition and II) a non-uniform displacement condition starting at zero at the top edge and linearly increasing to the bottom edge. The applied displacement magnitudes in load case II depend on the position of the nodes (and atoms) in the reference undeformed configuration.

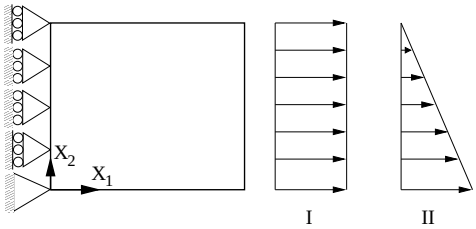

Figure 3 : Load conditions for examples. Load I is a uniform displacement conditions and Load II is non-uniform.

All degrees of freedom on the left edge of the sheet are constrained in the X_1 direction and are free in the X_2 direction. However, one degree of freedom in the X_2 direction is constrained to remove rigid body solutions. Applied displacements on the right edge of the sheet are applied in increments. All results are for quasistatically applied displacement increments. This means that nonlinear iterations are performed in each load increment until nodal displacements between iterations satisfy $|\mathbf{u}| = \sqrt{\mathbf{u}\cdot\mathbf{u}} < tol$ where the tolerance tol is set to $tol = 10^{-10}$Å. For the molecular dynamics, the atoms are quenched with each incremental displacement. This is performed by setting a bath temperature to 200 K and cooling adiabatically for 250-1000 time steps of 10^{-16} seconds each. The quenching process involves setting the velocity of an atom to zero whenever the energy of that atom rises above its value from the previous time step. The process continues until the total kinetic energy reaches a small tolerance value. For 1000 quenching steps the average tolerance is 3×10^{-6} eV, for 500 steps 2×10^{-5} eV, and for 250 steps 1×10^{-4} eV.

Two sheets of graphene one atom thick were tested. The first has 66 atoms and is depicted by Sheet A in Figure 4. The second has 1952 atoms and is depicted by Sheet B in Figure 5.

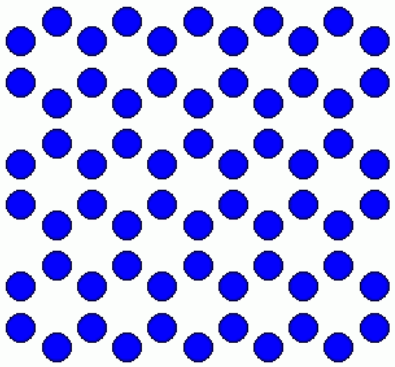

Figure 4 : Sheet A: Graphene with 66 atoms of dimensions 12.5632 Å$\times$ 11.6054 Å.

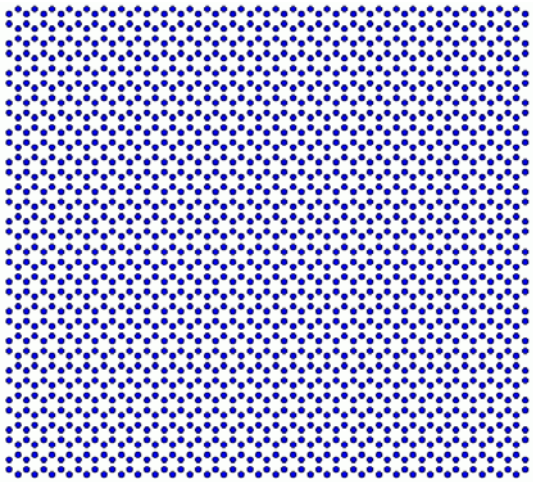

Figure 5 : Sheet B: Graphene with 1952 atoms of dimensions 75.3794 Å$\times$ 68.1819 Å.

Varying levels of mesh refinement were tested for both load conditions. The number of elements used in Sheet A are 4, 9, 16, and 25. The number of elements used for

Sheet B are 4, 36, 100, 225, 400, 625, and 900. The extent of the refinement is limited by the size restriction on each element established in equation (26). For the examples considered, each mesh is composed of quadrilateral elements. The local atom positions within each deformed element are interpolated using the isoparametric shape functions. The local position coordinates $(\eta_{1_\alpha}, \eta_{2_\alpha})$ and global position coordinates in the reference configuration $(X_{1_\alpha}, X_{2_\alpha})$ are related by

$$\begin{aligned} \eta_{1_\alpha} &= \frac{2}{L} X_{1_\alpha} - 1 \\ \eta_{2_\alpha} &= \frac{2}{W} X_{2_\alpha} - 1. \end{aligned} \tag{38}$$

where L and W are the element dimensions. Then, based on $(\eta_{1_\alpha}, \eta_{2_\alpha})$, the position coordinates in the deformed configuration $\mathbf{x}_\alpha = (x_{1_\alpha}, x_{2_\alpha})$ are given by

$$\mathbf{x}_\alpha = \sum_{a=1}^{4} N_a(\boldsymbol{\eta}_\alpha)\mathbf{x}_a. \tag{39}$$

6.1 Bulk Elastic Properties

Using the second derivative of the Tersoff-Brenner potential, the bulk values for the first Lagrangian elasticity tensor (in units eV/atom) for graphene were computed,

$$C_{1111} = 66.51 \quad C_{2112} = 21.63, \tag{40}$$

$$C_{1122} = 20.06 \quad C_{2121} = 24.83, \tag{41}$$

$$C_{1212} = 24.83 \quad C_{2211} = 20.06, \tag{42}$$

$$C_{1221} = 21.63 \quad C_{2222} = 66.51, \tag{43}$$

and all remaining terms are zero. It is important to note that although the bulk properties for graphene possess several symmetry planes, the elements for the present methodology will not generally possess the same symmetries because the number of atoms in each element is much smaller than normally acceptable for bulk behavior and the atoms and nodes in general do not coincide. This also implies that the atom structure in each element is nonperiodic, a necessary feature needed to capture nonlocal behavior. The equilibrium energy is -7.37563 eV/atom and nearest neighbor bond length 1.4507 Å. For an assumed layer thickness of 3.4 Å, which is the standard layer separation thickness for graphite, the effective Young's modulus from the present calculation is $Y = 1.261$ TPa with an effective Poisson's ratio of 0.302. These values agree well with measured values for graphite and carbon nanotubes [Krishnan, Dujardin, Ebbesen, Yianilos, and Treacy (1998)].

6.2 Numerical Performance

Comparisons between load steps and iterations are shown in Table 2. Numerical tolerance or convergence is defined as the point where doubling the number of displacement increments (halving the size of each increment) changes the final energy of the system by less than 0.05%. The quench steps required in the molecular dynamics simulations to obtain the static configuration of the atoms are analogous with the nonlinear iterations that satisfy the convergence criteria above in the finite element method.

Table 2 : Displacement increments and quench steps needed for convergence at 20% strain.

	Displacement Increments	Quench Steps
Present	200	$\leq$10
MD	4000	250–1000

6.3 Strain Energy and Deformation Comparisons

Strain energies computed for Sheet A using Load Case I are shown for both the present finite element method and quenched MD in Figure 6. The results for 4, 9, 16, and 25 elements are indistinguishable at small strains (roughly $\leq$ 5%). No noticeable trends in the strain energies can be observed with refinement. At an edge displacement of approximately 3 Å, the finite element and quenched MD results diverge significantly. This is attributable to the larger cut-off zone used in the the MD simulations. Whereas the present finite element cut-off zone begins earlier and ranges between (1.7 Å, 2.0 Å), the MD cut-off zone ranges between (1.8 Å, 2.1 Å). The cut-off zones specify the ranges beyond which atom interactions are neglected. That is, any pair of atoms whose distance apart exceeds the range of the cut-off zone are omitted in the calculation of the potential. It is useful to note that 3 Å corresponds to approximately 25% strain which is far larger than conventionally accepted for the elastic regime and therefore presently indicates good agreement far into the inelastic regime.

The linear elastic curve is also shown for comparison. This result is equivalent to a straight application of the Cauchy-Born rule without iterating for the converged material response at each load step.

Strain energies for Sheet B using Load Case I are shown in Figure 7. Again, the mesh refinement produces no

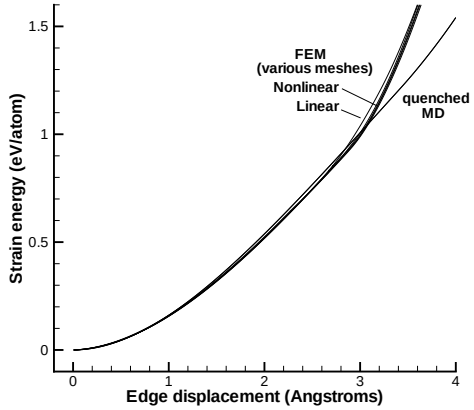

Figure 6 : Strain energy for Sheet A under Load Case I.

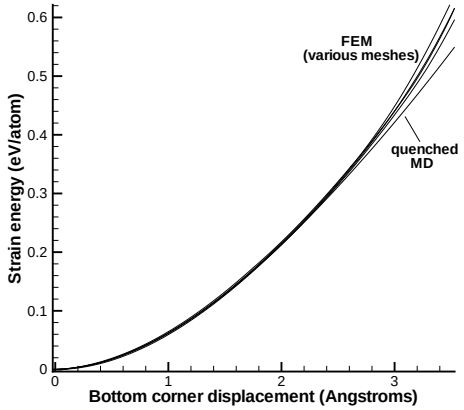

Figure 8 : Strain energy for Sheet A under Load Case II.

distinguishable differences among the different meshes, further demonstrating the viability of the present method for small scales. Also, as in Sheet A, the agreement in the elastic regime (roughly all strains smaller than 5%) is nearly exact, and shows excellent agreement up to approximately 25% strain. The linear result again also shows a stiffer response. This time, however, the difference is more pronounced because of the more complex interactions accompanying a problem with many more atoms.

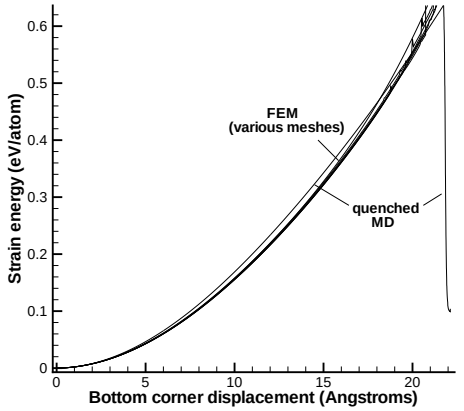

Figure 9 : Strain energy for Sheet B under Load Case II.

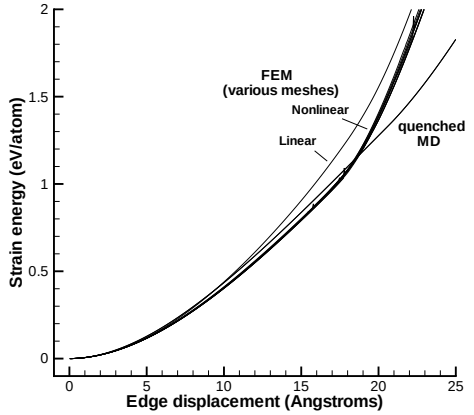

Figure 7 : Strain energy for Sheet B under Load Case I.

For the twisting deformations in Load Case II, the strain energy comparisons between finite elements and quenched MD are shown in Figures 8 and 9. As in Load Case I, differences at small strains are not noticeable.

The deformation shape for Sheet B under Load Case II at 21% elongation at the lower edge is shown in Figure 10 with the analogous atomistic solution in Figure 11.

At sufficiently large strain, the lower edge exhibits bond breaking which characterizes material failure. The present finite element method accurately predicts the bond breaking zone in a qualitative sense but does not predict the bond breaking itself. The inability to predict broken bonds is due to the assumption of the kinematic mapping scheme from equation (39). In the event of material failure, the atoms detach and create a free surface. Equation (39) prevents this from occuring by artificially forcing the atoms to remain in positions that have one-to-one correspondence with the original undeformed lattice. Therefore, it is envisioned that energetically acti-

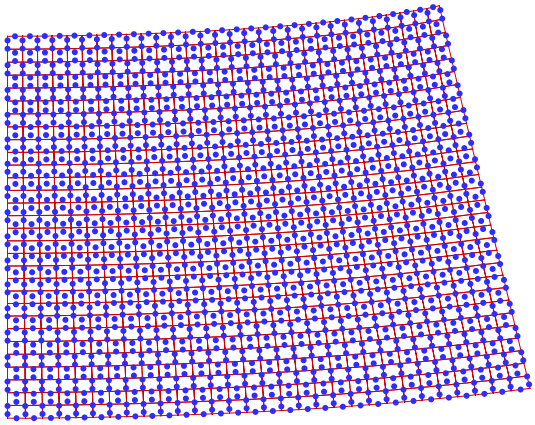

Figure 10 : Deformation configurations for finite elements and quenched MD at 21% elongation at the lower edge for Sheet B Load Case I. Mesh and lattice deformed configurations.

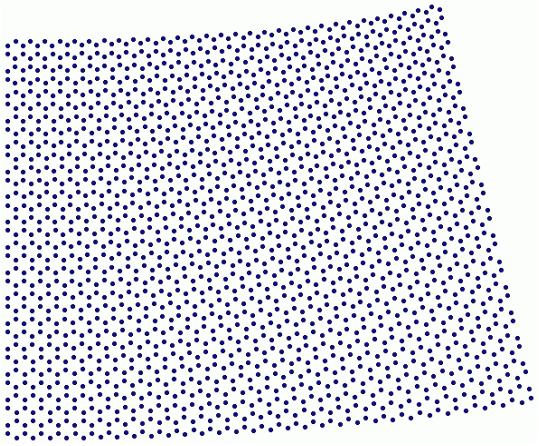

Figure 11 : Deformation configurations for finite elements and quenched MD at 21% elongation at the lower edge for Sheet B Load Case I. Quenched MD lattice in deformed configuration.

vated phenomena such as crack propagation cannot be modeled using the proposed approach. Instead, in regions where highly energetic processes occur, a molecular dynamics scheme at finite temperature with full atomistic resolution should be used.

Figure 12 shows the high strain region (showing $\sqrt{\mathbf{F}:\mathbf{F}}$) at 20% elongation at the lower edge. As the edge is further elongated, the strain magnitudes increase and the sheet of atoms begin to tear at this leading edge as depicted in Figure 13. At this extent of elongation, the finite element result has difficulty converging numerically.

It is of further interest to note that at the material failure event, the energy computed by finite elements discontinuously increases while the quenched MD result discontinuously decreases. The reason for this follows the explanation for the inability of finite elements to predict broken bonds. The isoparametric mapping scheme forces atoms that have debonded to remain unrealistically suspended, thus isolating them and creating an artificially high energy equivalent to the lattice dissociation energy of graphite. This leads to a very high energy being stored in the lattice and appears in a positive energy jump in the calculations. In reality, the material failure event creates two distinct surfaces with few or no atoms left suspended (this is an assumed quasistatic process) which has a far lower energy than a dissociated lattice. Hence this is characterized by a sudden energy decrease or energy release.

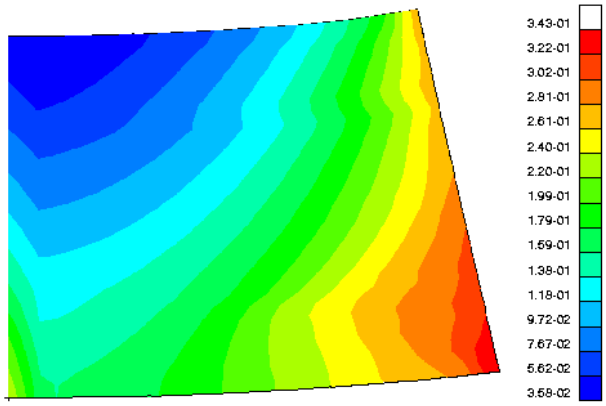

Figure 12 : Deformation magnitudes for Sheet B using 900 elements under Load Case II.

7 Discussion and Concluding Remarks

A finite element method based on lattice statics has been developed. Its purpose is to provide a computational mechanics framework for replacing small volumes (or areas) of atoms with a coarser finite element mesh. This capability is potentially useful in application for multiscale methods at the interface region, where continuum and atomistic domains are juxtaposed, and for estimating the mechanical response of very small scale devices.

The method provides several advantages over lattice statics or quenched molecular dynamics calculations. It creates a reduced number of degrees of freedom, which decreases the total number of equations to solve. An arbitrary reduction in the number of equations was tested

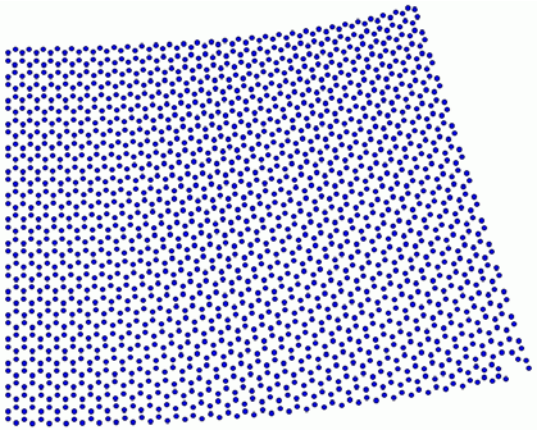

Figure 13 : Quenched MD simulation of sheet tearing. Bonds begin to break in lower right corner.

with different meshes and was found to yield accurate results for all refinements. The total number of nonlinear material iterations was found to be at least one order of magnitude smaller than the number of quenching steps needed in a molecular dynamics calculation to get the static configuration of the lattice. The size of each displacement increment was also allowed to be at least one order of magnitude larger than in the quenched MD simulations, allowing the lattice to reach its final configuration much faster.

As evidenced in the examples of small sheets of graphene under inhomogeneous deformation up to the moment of failure, the present method also provides insight into the mechanics of nanoscale devices. In a pseudo-linear regime where strains and deformation are very large (about 20% strain) but before gross material failure has occurred, the method is very accurate relative to the lattice statics calculations and even correctly predicts inhomogeneous strain patterns which sheds light on regions of potential atomistic/material failure. Adaptive techniques such as the quasicontinuum method [Tadmor, Ortiz, and Phillips (1996)] can then be applied to refine the calculations in these regions by substituting the element with more accurate molecular dynamics. The method may also be useful for studies of mechanical instabilities in nanotubes by predicting regions along the tube axis that are subject to buckling, kinking, or the like.

Some limitations of the method are also evident from the present study. Although the method correctly accounts for the material symmetries of the crystal because it is based on a finite element continuum method, it is not yet general enough to handle energy invariant deformations. That is, deformations that map the lattice onto itself, such as shear along a plane of atoms or along a stacking fault which require extensive gross deformation of the elements, cannot be considered using the present models alone. Such problems are the topics of numerous investigations currently underway.

Acknowledgement: The authors gratefully acknowledge the support by the U. S. Army Research Laboratory Director's Research Initiative (DRI) Program.

References

Arroyo, M.; Belytchko, T. (2002): An atomistic-based finite deformation membrane for crystalline films one atom thick. *Journal of the Mechanics and Physics of Solids*, vol. 50, no. 9, pp. 1941–1977.

Atluri, S. N. (1979): On rate principles for finite strain analysis of elastic and inelastic nonlinear solids. In *Recent Research on Mechanical Behavior*, pp. 79–107. University of Tokyo Press.

Atluri, S. N. (1980): On some new general and complementary energy theorems for the rate problems in finite strain, classical elastoplasticity. *Journal of Structural Mechanics*, vol. 8, no. 1, pp. 61–92.

Brenner, D. W. (1990): Empirical potential for hydrocarbons for use in simulating the chemical vapor deposition of diamond films. *Physical Review B*, vol. 42, no. 15, pp. 9458–9471.

Brenner, D. W.; Shenderova, O. A.; Areshkin, D. A.; Schall, J. D. (2002): Atomic modeling of carbon-based nanostructures as a tool for developing new materials and technologies. *CMES: Computer Modeling in Engineering & Sciences*, vol. 3, no. 5, pp. 643–674.

Broughton, J. Q.; Abraham, F. F.; Bernstein, N.; Kaxiras, E. (1999-II): Concurrent coupling of length scales: Methodology and application. *Physical Review B*, vol. 60, no. 4, pp. 2391–2403.

Chung, P. W.; Namburu, R. R. (2003): On a formulation for a multiscale atomistic-continuum homogenization method. *International Journal of Solids and Structures*, vol. 40, pp. 2563–2588.

DeLeeuw, S. W.; Perram, J. W.; Smith, E. R. (1980): Simulation of electrostatic systems in periodic boundary

conditions. i. lattice sums and dielectric constants. *Proceedings of the Royal Society of London A*, vol. 373, pp. 27–56.

Eberly, D. (2002): *Distance between point and triangle in 3D*. Magic Software (www.magic-software.com), 6006 Meadow Run Court, Chapel Hill, NC 27516, 2002.

Ericksen, J. L. (1984): *Phase Transformations and Material Instabilities in Solids*, pp. 61–77. Academic Press, Inc., 1984.

Ewald, P. (1921): Die berechnung optischer und elektrostatischer gitterpotentiale. *Annalen der Physik*, vol. 64, pp. 253–287.

Heyes, D. M. (1981): Electrostatic potentials and fields in infinite point charge lattices. *Journal of Chemical Physics*, vol. 74, pp. 1924–1929.

Knap, J.; Ortiz, M. (2001): An analysis of the quasicontinuum method. *Journal of the Mechanics and Physics of Solids*, vol. 49, pp. 1899–1923.

Kohlhoff, S.; Gumbsch, P.; Fischmeister, H. F. (1991): Crack propagation in b.c.c. crystals studied with a combined finite-element and atomistic model. *Philosophical Magazine A*, vol. 64, no. 4, pp. 851–878.

Krishnan, A.; Dujardin, E.; Ebbesen, T. W.; Yianilos, P. N.; Treacy, M. M. J. (1998): Young's modulus of single-walled nanotubes. *Physical Review B*, vol. 58, pp. 14013–14019.

Kroner, E. (1967): Elasticity theory of materials with long range cohesive forces. *International Journal of Solids and Structures*, vol. 3, pp. 731–742.

Madelung, E. (1918): Das elektrische feld in systemen von regalmässig angeordneten punktladungen. *Zeitschrift für Physik*, vol. 19, pp. 524–533.

Marsden, J. E.; Hughes, T. J. R. (1983): *Mathematical Foundations of Elasticity*. Dover Publications, Inc., New York.

Mullins, M.; Dokainish, M. A. (1982): Simulation of the (001) plane crack in α-iron employing a new boundary scheme. *Philosophical Magazine A*, vol. 46, pp. 771–787.

Ngo, N. D.; Tamma, K. K. (2004): An integrated comprehensive approach to the modeling of resin transfer molded composite manufactured net-shaped parts. *CMES: Computer Modeling in Engineering & Sciences*, vol. 5, no. 2, pp. 103–133.

Noguchi, H.; Furuya, Y. (1997): A method of seamlessly combining a crack tip molecular dynamics enclave with a linear elastic outer domain in simulating elastic-plastic crack advance. *International Journal of Fracture*, vol. 87, pp. 309–329.

Okada, H.; Fukui, Y.; Kumazawa, N. (2004): Homogenization Analysis for Particulate Composite Materials Using the Boundary Element Method, *CMES: Computer Modeling in Engineering & Sciences*, vol. 5, no. 2, pp. 135–149.

Raghavan, P.; Ghosh, S. (2004): An adaptive multi-level computational model for composite laminates. *CMES: Computer Modeling in Engineering & Sciences*, vol. 5, no. 2, pp. 151–170.

Rifkin, J. (2002): *XMD - Molecular Dynamics Program User Manual*. Center for Materials Simulations, Institute of Materials Science, University of Connecticut, 2002.

Shenoy, V. B. (1999): *Quasicontinuum Models of Atomic-Scale Mechanics*. PhD thesis, Brown University, 1999.

Sinclair, J. (1971): Improved atomistic model of a bcc dislocation core. *Journal of Applied Physics*, vol. 42, pp. 5321–5329.

Tadmor, E. B.; Ortiz, M.; Phillips, R. (1996): Quasicontinuum analysis of defects in solids. *Philosophical Magazine A*, vol. 73, no. 6, pp. 1529–1563.

Tersoff, J. (1988): Empirical interatomic potential for carbon, with applications to amorphous carbon. *Physical Review Letters*, vol. 61, no. 25, pp. 2879–2882.

Wong, E. W.; Sheehan, P. E.; Lieber, C. M. (1997): Nanobeam mechanics: Elasticity, strength and toughness of nanorods and nanotubes. *Science*, vol. 277, pp. 1971–1975.

Yakobson, B. I.; Brabec, C. J.; Bernholc, J. (1996): Nanomechanics of carbon tubes: Instabilities beyond linear response. *Physical Review Letters*, vol. 76, pp. 2511–2514.

Appendix A: Derivatives of the Tersoff-Brenner Potential

The derivatives needed to form the first Piola-Kirchoff stress and first Lagrangian elasticity tensor are shown here in detail. To simplify the notation, we define the following expressions,

$$r_{(ij)} = \left|\mathbf{r}_{(ij)}\right|, \tag{44}$$

$$f'_{(ij)}(r) = \frac{\partial f_{(ij)}}{\partial r_{(ij)}} \qquad f''_{(ij)}(r) = \frac{\partial^2 f_{(ij)}}{\partial r^2_{(ij)}}. \tag{45}$$

Note that although the equations are written in component form with respect to atoms, it is still in dyadic notation due to the multi-axial components of $\mathbf{r}_{(ij)}$. That is $r_{(ij)} \cdot \mathbf{e}_1$ is the component of the vector originating at atom i and terminating at atom j in the direction of $\mathbf{e}_1$, $r_{(ij)} \cdot \mathbf{e}_2$ is the component in the direction of $\mathbf{e}_2$, etc. From equations (17)–(22), the derivatives in equation (35) are defined by

$$\frac{\partial E_b}{\partial \mathbf{r}_{(ij)}} = \sum_i \sum_{j(>i)} \left[V'_R \frac{\partial r_{(ij)}}{\partial \mathbf{r}_{(ij)}} - V_A \frac{\partial \overline{B}}{\partial \mathbf{r}_{(ij)}} - \overline{B} V'_A \frac{\partial r_{(ij)}}{\partial \mathbf{r}_{(ij)}} \right], \tag{46}$$

$$\frac{\partial E_b}{\partial \mathbf{r}_{(ik)}} = \sum_i \sum_{j(>i)} \left[-V_A \frac{\partial \overline{B}}{\partial \mathbf{r}_{(ik)}} \right], \tag{47}$$

$$\frac{\partial E_b}{\partial \mathbf{r}_{(jk)}} = \sum_i \sum_{j(>i)} \left[-V_A \frac{\partial \overline{B}}{\partial \mathbf{r}_{(jk)}} \right], \tag{48}$$

$$\frac{\partial V_R}{\partial r_{(ij)}} = V'_R = f'_{(ij)} \frac{D^{(e)}}{(S-1)} e^{-\alpha_1 (r_{(ij)} - R^{(e)})} - \alpha_1 \frac{f_{(ij)} D^{(e)}}{(S-1)} e^{-\alpha_1 (r_{(ij)} - R^{(e)})}, \tag{49}$$

$$\frac{\partial V_A}{\partial r_{(ij)}} = V'_A = f'_{(ij)} \frac{D^{(e)} S}{(S-1)} e^{-\alpha_2 (r_{(ij)} - R^{(e)})} - \alpha_2 \frac{f_{(ij)} D^{(e)} S}{(S-1)} e^{-\alpha_2 (r_{(ij)} - R^{(e)})}, \tag{50}$$

$$\frac{\partial \overline{B}}{\partial \mathbf{r}_{(ij)}} = \frac{1}{2} \left\{ -\delta B^{1+\frac{1}{\delta}}_{(ij)} \sum_{k \neq (i,j)} \left[\frac{\partial G(\theta_{(ijk)})}{\partial \mathbf{r}_{(ij)}} f_{(ik)} \right] - \delta B^{1+\frac{1}{\delta}}_{(ji)} \sum_{k \neq (i,j)} \left[\frac{\partial G(\theta_{(jik)})}{\partial \mathbf{r}_{(ij)}} f_{(ik)} \right] \right\}, \tag{51}$$

$$\frac{\partial \overline{B}}{\partial \mathbf{r}_{(ik)}} = -\frac{\delta}{2} B^{1+\frac{1}{\delta}}_{(ij)} \sum_{k \neq (i,j)} \left[\frac{\partial G(\theta_{(ijk)})}{\partial \mathbf{r}_{(ik)}} f_{(ik)} + G(\theta_{(ijk)}) f'_{(ik)} \frac{\partial r_{(ik)}}{\partial \mathbf{r}_{(ik)}} \right], \tag{52}$$

$$\frac{\partial \overline{B}}{\partial \mathbf{r}_{(jk)}} = -\frac{\delta}{2} B^{1+\frac{1}{\delta}}_{(ji)} \sum_{k \neq (i,j)} \left[\frac{\partial G(\theta_{(jik)})}{\partial \mathbf{r}_{(jk)}} f_{jk} + G(\theta_{(jik)}) f'_{jk} \frac{\partial r_{(jk)}}{\partial \mathbf{r}_{(jk)}} \right], \tag{53}$$

$$\frac{\partial G(\theta_\gamma)}{\partial \mathbf{r}_{(mn)}} = \frac{2 a_o c_o^2 (1 + \cos\theta_\gamma)}{\left[d_o^2 + (1 + \cos\theta_\gamma)^2 \right]^2} \frac{\partial \cos\theta_\gamma}{\partial \mathbf{r}_{(mn)}}, \tag{54}$$

for $(mn) = (ij), (ik)$ when $\gamma = (ijk)$ and $(mn) = (ij), (jk)$ when $\gamma = (jik)$. The angles $\theta_{(ijk)}$ and $\theta_{(jik)}$, shown in Figure 14, are the angles subtending the connecting lines at the atoms i and j, respectively. Note that $\mathbf{r}_{(ij)} = -\mathbf{r}_{(ji)}$. The following identities can also be shown

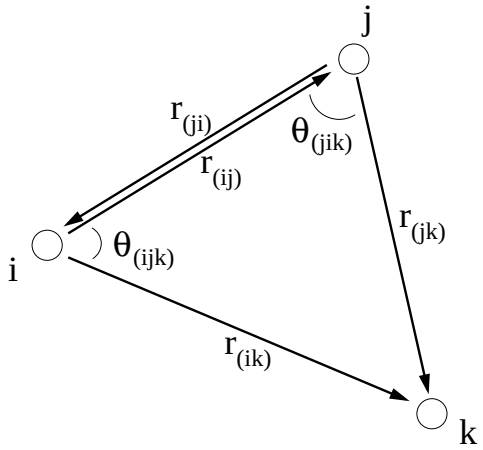

Figure 14 : Angles and inter-atom vectors.

$$\frac{\partial r_{(ij)}}{\partial \mathbf{r}_{(ij)}} = \frac{\partial (\mathbf{r}_{(ij)} \cdot \mathbf{r}_{(ij)})^{1/2}}{\partial \mathbf{r}_{(ij)}} = \frac{1}{2} \frac{1}{r_{(ij)}} 2 \mathbf{r}_{(ij)} = \frac{\mathbf{r}_{(ij)}}{r_{(ij)}}, \tag{55}$$

$$\frac{\partial \cos\theta_{(ijk)}}{\partial \mathbf{r}_{(ij)}} = \frac{\partial}{\partial \mathbf{r}_{(ij)}} \left(\frac{\mathbf{r}_{(ij)} \cdot \mathbf{r}_{(ik)}}{r_{(ij)} r_{(ik)}} \right) = \frac{\mathbf{r}_{(ik)}}{r_{(ij)} r_{(ik)}} - \frac{\mathbf{r}_{(ij)}}{r^2_{(ij)}} \cos\theta_{(ijk)}, \tag{56}$$

$$\frac{\partial \cos\theta_{(ijk)}}{\partial \mathbf{r}_{(ik)}} = \frac{\mathbf{r}_{(ij)}}{r_{(ij)} r_{(ik)}} - \frac{\mathbf{r}_{(ik)}}{r^2_{(ik)}} \cos\theta_{(ijk)}, \tag{57}$$

$$\frac{\partial \cos\theta_{(jik)}}{\partial \mathbf{r}_{(ij)}} = -\frac{\mathbf{r}_{(jk)}}{r_{(ji)} r_{(jk)}} + \frac{\mathbf{r}_{(ji)}}{r^2_{(ji)}} \cos\theta_{(jik)}, \tag{58}$$

$$\frac{\partial \cos\theta_{(jik)}}{\partial \mathbf{r}_{(jk)}} = \frac{\mathbf{r}_{(ji)}}{r_{(ji)} r_{(jk)}} - \frac{\mathbf{r}_{(jk)}}{r^2_{(jk)}} \cos\theta_{(jik)}. \tag{59}$$

It is important to note that

$$\frac{\partial \mathbf{r}_{(ij)}}{\partial \mathbf{q}_{(m)}} = \begin{cases} -\mathbf{I} & m = i \\ \mathbf{I} & m = j \\ \mathbf{0} & m \neq (i,j) \end{cases}, \tag{60}$$

where $\mathbf{I}$ is the 3×3 identity tensor for a system in a three dimensional domain. The derivative with respect to $\mathbf{r}_{(ik)}$ can be obtained likewise. This indicates that the summations in equations (46), (47), (51), and (52), when multiplied by (60) in (35) are nontrivial if and only if m is equal to i, j, or k.

For the first Lagrangian elasticity tensor in equation (36), the differential terms are defined by,

$$\begin{aligned}\frac{\partial^2 E_b}{\partial \mathbf{r}_{(ij)}\partial \mathbf{r}_{(ij)}} =& \sum_i \sum_{j(>i)} \left[\left(V_R'' - \overline{B} V_A'' \right) \left(\frac{\partial r_{(ij)}}{\partial \mathbf{r}_{(ij)}} \otimes \frac{\partial r_{(ij)}}{\partial \mathbf{r}_{(ij)}} \right) \right. \\ & + V_A' \frac{\partial^2 r_{(ij)}}{\partial \mathbf{r}_{(ij)}\partial \mathbf{r}_{(ij)}} - V_A' \left(\frac{\partial \overline{B}}{\partial \mathbf{r}_{(ij)}} \otimes \frac{\partial r_{(ij)}}{\partial \mathbf{r}_{(ij)}} \right) \\ & \left. - V_A \frac{\partial^2 \overline{B}}{\partial \mathbf{r}_{(ij)}\partial \mathbf{r}_{(ij)}} - V_A' \left(\frac{\partial r_{(ij)}}{\partial \mathbf{r}_{(ij)}} \otimes \frac{\partial \overline{B}}{\partial \mathbf{r}_{(ij)}} \right) \right], \end{aligned} \tag{61}$$

$$\begin{aligned}\frac{\partial^2 E_b}{\partial \mathbf{r}_{(ij)}\partial \mathbf{r}_{(ik)}} =& \sum_i \sum_{j(>i)} \left[-V_A' \left(\frac{\partial \overline{B}}{\partial \mathbf{r}_{(ik)}} \otimes \frac{\partial r_{(ij)}}{\partial \mathbf{r}_{(ij)}} \right) \right. \\ & \left. - V_A \frac{\partial^2 \overline{B}}{\partial \mathbf{r}_{(ij)}\partial \mathbf{r}_{(ik)}} \right], \end{aligned} \tag{62}$$

$$\begin{aligned}\frac{\partial^2 E_b}{\partial \mathbf{r}_{(ik)}\partial \mathbf{r}_{(ij)}} =& \sum_i \sum_{j(>i)} \left[-V_A' \left(\frac{\partial r_{(ij)}}{\partial \mathbf{r}_{(ij)}} \otimes \frac{\partial \overline{B}}{\partial \mathbf{r}_{(ik)}} \right) \right. \\ & \left. - V_A \frac{\partial^2 \overline{B}}{\partial \mathbf{r}_{(ik)}\partial \mathbf{r}_{(ij)}} \right], \end{aligned} \tag{63}$$

$$\frac{\partial^2 E_b}{\partial \mathbf{r}_{(ik)}\partial \mathbf{r}_{(ik)}} = \sum_i \sum_{j(>i)} \left[-V_A \frac{\partial^2 \overline{B}}{\partial \mathbf{r}_{(ik)}\partial \mathbf{r}_{(ik)}} \right], \tag{64}$$

$$\frac{\partial^2 E_b}{\partial \mathbf{r}_{(jk)}\partial \mathbf{r}_{(jk)}} = \sum_i \sum_{j(>i)} \left[-V_A \frac{\partial^2 \overline{B}}{\partial \mathbf{r}_{(jk)}\partial \mathbf{r}_{(jk)}} \right], \tag{65}$$

$$\begin{aligned}\frac{\partial^2 E_b}{\partial \mathbf{r}_{(ij)}\partial \mathbf{r}_{(jk)}} =& \sum_i \sum_{j(>i)} \left[-V_A' \left(\frac{\partial r_{(ij)}}{\partial \mathbf{r}_{(ij)}} \otimes \frac{\partial \overline{B}}{\partial \mathbf{r}_{(jk)}} \right) \right. \\ & \left. - V_A \frac{\partial^2 \overline{B}}{\partial \mathbf{r}_{(ij)}\partial \mathbf{r}_{(jk)}} \right], \end{aligned} \tag{66}$$

$$\begin{aligned}\frac{\partial^2 E_b}{\partial \mathbf{r}_{(jk)}\partial \mathbf{r}_{(ij)}} =& \sum_i \sum_{j(>i)} \left[-V_A' \left(\frac{\partial \overline{B}}{\partial \mathbf{r}_{(jk)}} \otimes \frac{\partial r_{(ij)}}{\partial \mathbf{r}_{(ij)}} \right) \right. \\ & \left. - V_A \frac{\partial^2 \overline{B}}{\partial \mathbf{r}_{(jk)}\partial \mathbf{r}_{(ij)}} \right], \end{aligned} \tag{67}$$

$$\frac{\partial^2 E_b}{\partial \mathbf{r}_{(ik)}\partial \mathbf{r}_{(jk)}} = \sum_i \sum_{j(>i)} \left[-V_A \frac{\partial^2 \overline{B}}{\partial \mathbf{r}_{(ik)}\partial \mathbf{r}_{(jk)}} \right], \tag{68}$$

$$\frac{\partial^2 E_b}{\partial \mathbf{r}_{(jk)}\partial \mathbf{r}_{(ik)}} = \sum_i \sum_{j(>i)} \left[-V_A \frac{\partial^2 \overline{B}}{\partial \mathbf{r}_{(jk)}\partial \mathbf{r}_{(ik)}} \right], \tag{69}$$

and additional algebra yields,

$$\begin{aligned} V_R'' = \frac{\partial^2 V_R}{\partial r_{(ij)}\partial r_{(ij)}} =& \left[\frac{f_{(ij)}'' D^{(e)}}{(S-1)} - \frac{2\alpha_1 f_{(ij)}' D^{(e)}}{(S-1)} \right. \\ & \left. + \frac{\alpha_1^2 f_{(ij)} D^{(e)}}{(S-1)} \right] e^{-\alpha_1 (r_{(ij)} - R^{(e)})}, \end{aligned} \tag{70}$$

$$\begin{aligned} V_A'' = \frac{\partial^2 V_A}{\partial r_{(ij)}\partial r_{(ij)}} =& \left[\frac{f_{(ij)}'' D^{(e)} S}{(S-1)} - \frac{2\alpha_2 f_{(ij)}' D^{(e)} S}{(S-1)} \right. \\ & \left. + \frac{\alpha_2^2 f_{(ij)} D^{(e)} S}{(S-1)} \right] e^{-\alpha_2 (r_{(ij)} - R^{(e)})}, \end{aligned} \tag{71}$$

$$\begin{aligned} & \frac{\partial^2 \overline{B}}{\partial \mathbf{r}_{(ij)}\partial \mathbf{r}_{(ij)}} \\ & = -\frac{(\delta+1)}{2} B_{(ij)}^{\frac{1}{\delta}} \sum_{k\neq(i,j)} f_{(ik)} \left(\frac{\partial G(\theta_{(ijk)})}{\partial \mathbf{r}_{(ij)}} \otimes \frac{\partial B_{(ij)}}{\partial \mathbf{r}_{(ij)}} \right) \\ & \quad - \frac{\delta}{2} B_{(ij)}^{1+\frac{1}{\delta}} \sum_{k\neq(i,j)} \left(f_{(ik)} \frac{\partial^2 G(\theta_{(ijk)})}{\partial \mathbf{r}_{(ij)}\partial \mathbf{r}_{(ij)}} \right) \\ & \quad - \frac{(\delta+1)}{2} B_{(ji)}^{\frac{1}{\delta}} \sum_{k\neq(i,j)} f_{jk} \left(\frac{\partial G(\theta_{(jik)})}{\partial \mathbf{r}_{(ij)}} \otimes \frac{\partial B_{(ji)}}{\partial \mathbf{r}_{(ij)}} \right) \\ & \quad - \frac{\delta}{2} B_{(ji)}^{1+\frac{1}{\delta}} \sum_{k\neq(i,j)} \left(f_{jk} \frac{\partial^2 G(\theta_{(jik)})}{\partial \mathbf{r}_{(ij)}\partial \mathbf{r}_{(ij)}} \right) \end{aligned} \tag{72}$$

$$\begin{aligned} & \frac{\partial^2 \overline{B}}{\partial \mathbf{r}_{(ij)}\partial \mathbf{r}_{(ik)}} \\ & = -\frac{(\delta+1)}{2} B_{(ij)}^{\frac{1}{\delta}} \sum_{k\neq(i,j)} \left[f_{(ik)} \left(\frac{\partial G(\theta_{(ijk)})}{\partial \mathbf{r}_{(ik)}} \otimes \frac{\partial B_{(ij)}}{\partial \mathbf{r}_{(ij)}} \right) \right. \\ & \qquad \left. + G(\theta_{(ijk)}) f_{(ik)}' \left(\frac{\partial r_{(ik)}}{\partial \mathbf{r}_{(ik)}} \otimes \frac{\partial B_{(ij)}}{\partial \mathbf{r}_{(ij)}} \right) \right] \\ & \quad - \frac{\delta}{2} B_{(ij)}^{1+\frac{1}{\delta}} \sum_{k\neq(i,j)} \left[f_{(ik)} \frac{\partial^2 G(\theta_{(ijk)})}{\partial \mathbf{r}_{(ij)}\partial \mathbf{r}_{(ik)}} \right. \\ & \qquad \left. + f_{(ik)}' \left(\frac{\partial r_{(ik)}}{\partial \mathbf{r}_{(ik)}} \otimes \frac{\partial G(\theta_{(ijk)})}{\partial \mathbf{r}_{(ij)}} \right) \right], \end{aligned} \tag{73}$$

$$
\begin{aligned}
&\frac{\partial^2 \overline{B}}{\partial \mathbf{r}_{(ik)} \partial \mathbf{r}_{(ij)}} \\
&= -\frac{(\delta+1)}{2} B_{(ij)}^{\frac{1}{\delta}} \sum_{k \neq (i,j)} \left[f_{(ik)} \left(\frac{\partial G(\theta_{(ijk)})}{\partial \mathbf{r}_{(ij)}} \otimes \frac{\partial B_{(ij)}}{\partial \mathbf{r}_{(ik)}} \right) \right] \\
&\quad - \frac{\delta}{2} B_{(ij)}^{1+\frac{1}{\delta}} \sum_{k \neq (i,j)} \left[f_{(ik)} \frac{\partial^2 G(\theta_{(ijk)})}{\partial \mathbf{r}_{(ik)} \partial \mathbf{r}_{(ij)}} \right. \\
&\qquad \left. + f'_{(ik)} \left(\frac{\partial G(\theta_{(ijk)})}{\partial \mathbf{r}_{(ij)}} \otimes \frac{\partial r_{(ik)}}{\partial \mathbf{r}_{(ik)}} \right) \right],
\end{aligned} \tag{74}
$$

$$
\begin{aligned}
&\frac{\partial^2 \overline{B}}{\partial \mathbf{r}_{(ik)} \partial \mathbf{r}_{(ik)}} \\
&= -\frac{(\delta+1)}{2} B_{(ij)}^{\frac{1}{\delta}} \sum_{k \neq (i,j)} \left[f_{(ik)} \left(\frac{\partial G(\theta_{(ijk)})}{\partial \mathbf{r}_{(ik)}} \otimes \frac{\partial B_{(ij)}}{\partial \mathbf{r}_{(ik)}} \right) \right. \\
&\qquad \left. + G(\theta_{(ijk)}) f'_{(ik)} \left(\frac{\partial r_{(ik)}}{\partial \mathbf{r}_{(ik)}} \otimes \frac{\partial B_{(ij)}}{\partial \mathbf{r}_{(ik)}} \right) \right] \\
&\quad - \frac{\delta}{2} B_{(ij)}^{1+\frac{1}{\delta}} \sum_{k \neq (i,j)} \left[f_{(ik)} \frac{\partial^2 G(\theta_{(ijk)})}{\partial \mathbf{r}_{(ik)} \partial \mathbf{r}_{(ik)}} \right. \\
&\qquad + 2 f'_{(ik)} \left(\frac{\partial r_{(ik)}}{\partial \mathbf{r}_{(ik)}} \otimes \frac{\partial G(\theta_{(ijk)})}{\partial \mathbf{r}_{(ik)}} \right) \\
&\qquad + G(\theta_{(ijk)}) f''_{(ik)} \left(\frac{\partial r_{(ik)}}{\partial \mathbf{r}_{(ik)}} \otimes \frac{\partial r_{(ik)}}{\partial \mathbf{r}_{(ik)}} \right) \\
&\qquad \left. + G(\theta_{(ijk)}) f'_{(ik)} \frac{\partial^2 r_{(ik)}}{\partial \mathbf{r}_{(ik)} \partial \mathbf{r}_{(ik)}} \right].
\end{aligned} \tag{75}
$$

$$
\begin{aligned}
&\frac{\partial^2 \overline{B}}{\partial \mathbf{r}_{(ij)} \partial \mathbf{r}_{(jk)}} \\
&= -\frac{(\delta+1)}{2} B_{(ji)}^{\frac{1}{\delta}} \sum_{k \neq (i,j)} \left[f_{jk} \left(\frac{\partial G(\theta_{(jik)})}{\partial \mathbf{r}_{(jk)}} \otimes \frac{\partial B_{(ji)}}{\partial \mathbf{r}_{(ij)}} \right) \right. \\
&\qquad \left. + G(\theta_{(jik)}) f'_{jk} \left(\frac{\partial r_{(jk)}}{\partial \mathbf{r}_{(jk)}} \otimes \frac{\partial B_{(ji)}}{\partial \mathbf{r}_{(ij)}} \right) \right] \\
&\quad - \frac{\delta}{2} B_{(ji)}^{1+\frac{1}{\delta}} \sum_{k \neq (i,j)} \left[f_{jk} \frac{\partial^2 G(\theta_{(jik)})}{\partial \mathbf{r}_{(ij)} \partial \mathbf{r}_{(jk)}} \right. \\
&\qquad \left. + f'_{jk} \left(\frac{\partial G(\theta_{(jik)})}{\partial \mathbf{r}_{(jk)}} \otimes \frac{\partial r_{(jk)}}{\partial \mathbf{r}_{(ij)}} \right) \right],
\end{aligned} \tag{76}
$$

$$
\begin{aligned}
&\frac{\partial^2 \overline{B}}{\partial \mathbf{r}_{(jk)} \partial \mathbf{r}_{(ij)}} \\
&= -\frac{(\delta+1)}{2} B_{(ji)}^{\frac{1}{\delta}} \sum_{k \neq (i,j)} \left[f_{jk} \left(\frac{\partial G(\theta_{(jik)})}{\partial \mathbf{r}_{(ij)}} \otimes \frac{\partial B_{(ji)}}{\partial \mathbf{r}_{(jk)}} \right) \right] \\
&\quad - \frac{\delta}{2} B_{(ji)}^{1+\frac{1}{\delta}} \sum_{k \neq (i,j)} \left[f_{jk} \frac{\partial^2 G(\theta_{(jik)})}{\partial \mathbf{r}_{(jk)} \partial \mathbf{r}_{(ij)}} \right. \\
&\qquad \left. + f'_{jk} \left(\frac{\partial G(\theta_{(jik)})}{\partial \mathbf{r}_{(ij)}} \otimes \frac{\partial r_{(jk)}}{\partial \mathbf{r}_{(jk)}} \right) \right],
\end{aligned} \tag{77}
$$

$$
\begin{aligned}
&\frac{\partial^2 \overline{B}}{\partial \mathbf{r}_{(jk)} \partial \mathbf{r}_{(jk)}} \\
&= -\frac{(\delta+1)}{2} B_{(ji)}^{\frac{1}{\delta}} \sum_{k \neq (i,j)} \left[f_{jk} \left(\frac{\partial G(\theta_{(jik)})}{\partial \mathbf{r}_{(jk)}} \otimes \frac{\partial B_{(ji)}}{\partial \mathbf{r}_{(jk)}} \right) \right. \\
&\qquad \left. + G(\theta_{(jik)}) f'_{jk} \left(\frac{\partial r_{(jk)}}{\partial \mathbf{r}_{(jk)}} \otimes \frac{\partial B_{(ji)}}{\partial \mathbf{r}_{(jk)}} \right) \right] \\
&\quad - \frac{\delta}{2} B_{(ji)}^{1+\frac{1}{\delta}} \sum_{k \neq (i,j)} \left[f_{jk} \frac{\partial^2 G(\theta_{(jik)})}{\partial \mathbf{r}_{(jk)} \partial \mathbf{r}_{(jk)}} \right. \\
&\qquad + 2 f'_{jk} \left(\frac{\partial r_{(jk)}}{\partial \mathbf{r}_{(jk)}} \otimes \frac{\partial G(\theta_{(jik)})}{\partial \mathbf{r}_{(jk)}} \right) \\
&\qquad + G(\theta_{(jik)}) f''_{jk} \left(\frac{\partial r_{(jk)}}{\partial \mathbf{r}_{(jk)}} \otimes \frac{\partial r_{(jk)}}{\partial \mathbf{r}_{(jk)}} \right) \\
&\qquad \left. + G(\theta_{(jik)}) f'_{jk} \frac{\partial^2 r_{(jk)}}{\partial \mathbf{r}_{(jk)} \partial \mathbf{r}_{(jk)}} \right],
\end{aligned} \tag{78}
$$

and finally,

$$
\frac{\partial^2 \overline{B}}{\partial \mathbf{r}_{(ik)} \partial \mathbf{r}_{(jk)}} = \frac{\partial^2 \overline{B}}{\partial \mathbf{r}_{(jk)} \partial \mathbf{r}_{(ik)}} = \mathbf{0}, \tag{79}
$$

$$
\frac{\partial^2 r_{(ij)}}{\partial \mathbf{r}_{(ij)} \partial \mathbf{r}_{(ij)}} = \frac{\mathbf{I}}{r_{(ij)}} - \frac{\mathbf{r}_{(ij)} \otimes \mathbf{r}_{(ij)}}{r_{(ij)}^3}. \tag{80}
$$

To complete the derivation, the following identities are

needed,

$$\begin{aligned}\frac{\partial^2 G}{\partial \mathbf{r}_{(mn)}\partial \mathbf{r}_{(pq)}} &= \left(\frac{-8a_o c_o^2(1+\cos\theta_\gamma)^2}{(d_o^2+(1+\cos\theta_\gamma)^2)^3}+\frac{2a_o c_o^2}{(d_o^2+(1+\cos\theta_\gamma)^2)^2}\right)\\ &\quad\times\left(\frac{\partial\cos\theta_\gamma}{\partial \mathbf{r}_{(pq)}}\otimes\frac{\partial\cos\theta_\gamma}{\partial \mathbf{r}_{(mn)}}\right)\\ &\quad+\frac{2a_o c_o^2(1+\cos\theta_\gamma)}{(d_o^2+(1+\cos\theta_\gamma)^2)^2}\frac{\partial^2\cos\theta_\gamma}{\partial \mathbf{r}_{(mn)}\partial \mathbf{r}_{(pq)}},\end{aligned} \tag{81}$$

with the appropriate combinations of $(mn,pq)=(ij,ij),(ij,ik),(ik,ij),(ik,ik)$ for $\gamma=ijk$ and $(mn,pq)=(ij,jk),(jk,ij),(jk,jk)$ for $\gamma=jik$, and,

$$\begin{aligned}\frac{\partial^2\cos\theta_{(ijk)}}{\partial \mathbf{r}_{(ij)}\partial \mathbf{r}_{(ij)}} &= -\frac{1}{r_{(ij)}^3 r_{(ik)}}\left(\mathbf{r}_{(ij)}\otimes\mathbf{r}_{(ik)}\right)\\ &\quad-\frac{\cos\theta_{(ijk)}\mathbf{I}}{r_{(ij)}^2}+\frac{3\cos\theta_{(ijk)}}{r_{(ij)}^4}\left(\mathbf{r}_{(ij)}\otimes\mathbf{r}_{(ij)}\right)\\ &\quad-\frac{1}{r_{(ij)}^3 r_{(ik)}}\left(\mathbf{r}_{(ik)}\otimes\mathbf{r}_{(ij)}\right),\end{aligned} \tag{82}$$

$$\begin{aligned}\frac{\partial^2\cos\theta_{(ijk)}}{\partial \mathbf{r}_{(ij)}\partial \mathbf{r}_{(ik)}} &= -\frac{1}{r_{(ij)}^3 r_{(ik)}}\left(\mathbf{r}_{(ij)}\otimes\mathbf{r}_{(ij)}\right)\\ &\quad-\frac{1}{r_{(ij)} r_{(ik)}^3}\left(\mathbf{r}_{(ik)}\otimes\mathbf{r}_{(ik)}\right)\\ &\quad+\frac{\cos\theta_{(ijk)}}{r_{(ij)}^2 r_{(ik)}^2}\left(\mathbf{r}_{(ik)}\otimes\mathbf{r}_{(ij)}\right)+\frac{\mathbf{I}}{r_{(ij)} r_{(ik)}},\end{aligned} \tag{83}$$

$$\begin{aligned}\frac{\partial^2\cos\theta_{(ijk)}}{\partial \mathbf{r}_{(ik)}\partial \mathbf{r}_{(ij)}} &= -\frac{1}{r_{(ij)}^3 r_{(ik)}}\left(\mathbf{r}_{(ij)}\otimes\mathbf{r}_{(ij)}\right)\\ &\quad-\frac{1}{r_{(ij)} r_{(ik)}^3}\left(\mathbf{r}_{(ik)}\otimes\mathbf{r}_{(ik)}\right)\\ &\quad+\frac{\cos\theta_{(ijk)}}{r_{(ij)}^2 r_{(ik)}^2}\left(\mathbf{r}_{(ij)}\otimes\mathbf{r}_{(ik)}\right)+\frac{\mathbf{I}}{r_{(ij)} r_{(ik)}},\end{aligned} \tag{84}$$

$$\begin{aligned}\frac{\partial^2\cos\theta_{(ijk)}}{\partial \mathbf{r}_{(ik)}\partial \mathbf{r}_{(ik)}} &= -\frac{1}{r_{(ij)} r_{(ik)}^3}\left(\mathbf{r}_{(ik)}\otimes\mathbf{r}_{(ij)}\right)\\ &\quad-\frac{\cos\theta_{(ijk)}\mathbf{I}}{r_{(ik)}^2}+\frac{3\cos\theta_{(ijk)}}{r_{(ik)}^4}\left(\mathbf{r}_{(ik)}\otimes\mathbf{r}_{(ik)}\right)\\ &\quad-\frac{1}{r_{(ij)} r_{(ik)}^3}\left(\mathbf{r}_{(ij)}\otimes\mathbf{r}_{(ik)}\right),\end{aligned} \tag{85}$$

$$\begin{aligned}\frac{\partial^2\cos\theta_{(jik)}}{\partial \mathbf{r}_{(ij)}\partial \mathbf{r}_{(ij)}} &= -\frac{1}{r_{(ji)}^3 r_{(jk)}}\left(\mathbf{r}_{(jk)}\otimes\mathbf{r}_{(ji)}\right)\\ &\quad+\frac{\cos\theta_{(jik)}\mathbf{I}}{r_{(ji)}^2}+\frac{3\cos\theta_{(jik)}}{r_{(ji)}^4}\left(\mathbf{r}_{(ji)}\otimes\mathbf{r}_{(ji)}\right)\\ &\quad-\frac{1}{r_{(ji)}^3 r_{(jk)}}\left(\mathbf{r}_{(ji)}\otimes\mathbf{r}_{(jk)}\right),\end{aligned} \tag{86}$$

$$\begin{aligned}\frac{\partial^2\cos\theta_{(jik)}}{\partial \mathbf{r}_{(ij)}\partial \mathbf{r}_{(jk)}} &= \frac{1}{r_{(ji)}^3 r_{(jk)}}\left(\mathbf{r}_{(ji)}\otimes\mathbf{r}_{(ji)}\right)\\ &\quad+\frac{1}{r_{(ji)} r_{(jk)}^3}\left(\mathbf{r}_{(jk)}\otimes\mathbf{r}_{(jk)}\right)\\ &\quad-\frac{\cos\theta_{(jik)}}{r_{(ji)}^2 r_{(jk)}^2}\left(\mathbf{r}_{(jk)}\otimes\mathbf{r}_{(ji)}\right)-\frac{\mathbf{I}}{r_{(ji)} r_{(jk)}},\end{aligned} \tag{87}$$

$$\begin{aligned}\frac{\partial^2\cos\theta_{(jik)}}{\partial \mathbf{r}_{(jk)}\partial \mathbf{r}_{(ji)}} &= \frac{1}{r_{(ji)}^3 r_{(jk)}}\left(\mathbf{r}_{(ji)}\otimes\mathbf{r}_{(ji)}\right)\\ &\quad+\frac{1}{r_{(ji)} r_{(jk)}^3}\left(\mathbf{r}_{(jk)}\otimes\mathbf{r}_{(jk)}\right)\\ &\quad-\frac{\cos\theta_{(jik)}}{r_{(ji)}^2 r_{(jk)}^2}\left(\mathbf{r}_{(ji)}\otimes\mathbf{r}_{(jk)}\right)-\frac{\mathbf{I}}{r_{(ji)} r_{(jk)}},\end{aligned} \tag{88}$$

$$\begin{aligned}\frac{\partial^2\cos\theta_{(jik)}}{\partial \mathbf{r}_{(jk)}\partial \mathbf{r}_{(jk)}} &= -\frac{1}{r_{(ji)} r_{(jk)}^3}\left(\mathbf{r}_{(ji)}\otimes\mathbf{r}_{(jk)}\right)\\ &\quad-\frac{\cos\theta_{(jik)}\mathbf{I}}{r_{(jk)}^2}+\frac{3\cos\theta_{(jik)}}{r_{(jk)}^4}\left(\mathbf{r}_{(jk)}\otimes\mathbf{r}_{(jk)}\right)\\ &\quad-\frac{1}{r_{(ji)} r_{(jk)}^3}\left(\mathbf{r}_{(jk)}\otimes\mathbf{r}_{(ji)}\right).\end{aligned} \tag{89}$$

This completes the derivatives of the potential.

Despite the relative algebraic complexity of the expressions, the calculations can be performed readily using computers. The algorithm is based on an additive assembly process by casting the equations in their equivalent matrix forms and then summing over all unique pairs and triples of atoms, which translates well to an iterative computational methodology.